Since January 2020 Elsevier has created a COVID-19 resource centre with free information in English and Mandarin on the novel coronavirus COVID-19. The COVID-19 resource centre is hosted on Elsevier Connect, the company's public news and information website.

Journal of Molecular Graphics and Modelling 104 (2021) 107834

Contents lists available at ScienceDirect

Journal of Molecular Graphics and Modelling

journal homepage: www.elsevier.com/locate/JMGM

A potential solution to avoid overdose of mixed drugs in the event of Covid-19: Nanomedicine at the heart of the Covid-19 pandemic

Eric Duverger [a], Guillaume Herlem [b], Fabien Picaud [b, *]

[a] FEMTO-ST Institute, Université Bourgogne Franche-Comté, CNRS, 15B avenue des Montboucons, F-25030, Besançon, Cedex, France
[b] Nanomedicine, Imagery and Therapeutics Lab, Université de Bourgogne Franche-Comté, 16 route de Gray, 25000, Besançon, France

ARTICLE INFO

Article history:
Received 12 August 2020
Received in revised form
18 December 2020
Accepted 30 December 2020
Available online 4 January 2021

Keywords:
Density functional theory calculations
Molecular dynamics simulations
Nanovectorization

ABSTRACT

Since 2020, the world is facing the first global pandemic of 21st century. Among all the solutions proposed to treat this new strain of coronavirus, named SARS-CoV-2, the vaccine seems a promising way but the delays are too long to be implemented quickly. In the emergency, a dual therapy has shown its effectiveness but has also provoked a set of debates around the dangerousness of a particular molecule, hydroxychloroquine. In particular, the doses to be delivered, according to the studies, were well beyond the acceptable doses to support the treatment without side effects. We propose here to use all the advantages of nanovectorization to address this question of concentration. Using quantum and classical simulations we will show in particular that drug transport on boron nitrogen oxide nanosheets increases the effectiveness of the action of these drugs. This will definitely allow to decrease the drug quantity needing to face the disease.

1. Introduction

Since the beginning of 2020, our world is completely upset by the appearance of a novel strain of coronavirus. On March 11th, the World Health Organization (WHO) declared a pandemic due to this COVID-19 (2019-nCoV). Coronaviruses (CoV) can cause several pulmonary diseases in mammals [1,2]. The first of these emerged in 2002 (called SARS-CoV) and was responsible for strong breathing syndromes leading to a mortality rate of 10%. The second virus (MERS-CoV) appeared in 2012 with a significantly higher virulence rate (mortality of about 35%). Fortunately, these two diseases had a low contagion rate (less than 100000 cases for the SARS-CoV) or remained very localized (only condensed in the Arabic peninsula for the MERS-CoV) and few deaths were recorded (less than 10000). However, these were the first alerts upon the apparition of a new strain of viruses.

The new virus originally named SARS-CoV-2 [3] due to its similarity to the SARS strain genome (about 82%) [4,5] was initially reported in Wuhan. Its amazing mode of human-to-human transmission has led to an explosive expansion in the number of cases, which has resulted in the virus spreading around the world. As of December 17, WHO had confirmed 72,851,747 cumulative cases and 1,643,339 deaths. The mortality rate tends thus to 2.3% but is very dependent on both health and age of the patient. However, the significant development of the virus in the southern hemisphere causes its important resurgence in the daily months, i.e. the famous second wave. And worse, this virus could become seasonal, raising the fear of its appearance each year, and therefore successive waves of a pandemic.

There is a huge challenge facing the whole scientific community, especially virologists, in finding a solution to this pandemic.

The structure of the SARS-Cov-2 virus consists of four structural domains. Its spherical envelope (around 100 nm diameter) is made of a nucleoprotein surrounded by a lipid bilayer coming from the host cell. This latter contains 3 other proteins: the membrane one (M), the envelope one (E) and the spike one (S) [6]. The latter (S) is responsible for binding the virus to the host cell and the fusion of the protein [7,8]. When homotrimerized, it causes viral infection through two domains. The S1 domain, which contains the receptor binding domain (or RBD) aims to bind to the host cell receptor [9], also known as angiotensin converting enzyme 2 (ACE-2) [10]. The S2 domain is responsible for fusion of protein E with the host cell [11].

In recent years, drug development process against emerging viral infection has been increased and assisted by the amazing explosion of computer resources. The repurposing methodology

* Corresponding author. Nanomedicine, Imagery and Therapeutics Lab, Université de Bourgogne Franche-Comté, 16 route de Gray, 25000, Besançon, France.
E-mail address: fabien.picaud@univ-fcomte.fr (F. Picaud).

https://doi.org/10.1016/j.jmgm.2021.107834
1093-3263/

[12] has led to the discovery of several therapeutics agents against diseases such as Ebola, or hepatitis C virus [13,14].

Recent calculations have been performed on SARS-CoV-2 [15] using clinically approved drugs such as Lopinavir−Ritonavir [16]. However, clinical trials have not been convincing and therefore have limited the use of these drugs by hospital settings. In parallel, some hospitals have used a dual therapeutic treatment comprising both azythromicin (AZM) and hydroxychloroquine (HCQ) molecules. The efficiency of this association of an antibiotic and an antimalarial was found to be high if the drugs were given in the initial state of the disease and with a normal dose. Conversely, when given at the early stage of the disease (and with higher doses), side effects (namely the cardiac problems) lead to an increased mortality rate.

In recent years, nanomedicine has experienced significant development since it allows drugs to be delivered at the targeted cell. Using nanovectors such as nanotubes (of different constitutions) [17−21] or nanoflakes (of different constitutions) [22,23], researchers can now safely transport drug molecules to their target and attack only the diseased part organs. Among the great diversity of nanovectors, boron nitride oxide nanoflakes (BNO) have recently attracted particular interest due to their bio human compatibility [24,25]. Herein, in order to answer to the difficult question of the medical dose of each drug in the treatment of SARS-CoV-2, we will study in this paper the transport of HCQ or AZM (or both) using BNO towards the receptor binding of the virus or the closed state structure of the viral protein.

The paper is organized as follows. After describing the numerical methods used in this paper, we will study the stability of the nanovector using quantum simulations. Then, the nanovectorization of each drug will be studied to demonstrate its ability to target the viral protein. If successful, this novel technology could answer to the difficult question of medical doses since the vector would improve the accessibility of the drug until its target.

2. Computational method

2.1. Density functional theory

To simulate the adsorption of Azythromicin **(**AZM**)**, Hydroxychloroquine **(**HCQ**)** and to study the nature of the interactions between these molecules and boron nitride oxide **(**BNO**)** nanoflakes, theoretical approach based on density functional theory (DFT) method has been used thanks to the SIESTA code [26−29]. The calculations were carried out using a polarized double ζ basis set (DZP), non-local norm conserving pseudopotentials and, for the exchange correlation functional, in all calculations, we used the generalized gradient approximation (GGA) including the van der Waals interaction [30−32]. The mesh cutoff of 150 Ry with a single k-point at the center Γ for the Brillouin zone integration was considered to calculate the total energies within a numerical precision of 1 meV. Geometry relaxation was performed by the conjugate-gradient method with the force convergence criterion of 0.02 eV/Å in the same slab volume (i.e., $4 \times 4 \times 4$ nm^3). AZM as depicted in Fig. 1-a ($C_{38}H_{72}N_2O_{12}$) as well as HCQ ($C_{18}H_{26}ClN_3O$) in Fig. 1-b and BNO (Fig. 1-c, 1-d) were fully optimized separately under vacuum in a first step. BNO ($N_{38}B_{38}O_{22}H_{36}$) contained hydroxyl radicals (-OH) and oxo bridges (O) distributed randomly on both faces as reported in the literature [33−37]. Hydrogen atoms were added on edge atoms to avoid dangling bond effects.

In a second step, we studied three different molecule/BNO systems shown in Fig. 2: AZM/BNO, HCQ/BNO and AZM/BNO/HCQ. In order to determine the best conformational/adsorption energy, SIESTA DFT molecular dynamic simulation was performed in vacuum. The initial configurations were calculated by random placements of the molecule on BNO. Then, energy minimizations were performed on the system via a position relaxation calculation to obtain an optimized configuration of the molecule and the nanoflake. We then determine the adsorption energy (E_{ads}) to verify the stability of the molecule(s) adsorbed on BNO. E_{ads} was calculated using the following equation:

$$E_{ads} = E(\text{Molecule(s)} + \text{BNO}) - E(\text{BNO}) - E(\text{Molecule(s)})$$

E(Molecule(s) + BNO) is the total energy of molecule(s) adsorbed on BNO after energetic relaxation of its geometry in vacuum. E(BNO) and E(Molecule(s)) are respectively the energy of the optimized nanoflake and of the molecule(s). $E_{ads} < 0$ corresponds to stable adsorption on the nanoflake. The charge distributions between molecules and the BNO surface were analyzed using the Bader approach [38,39] and used as them in the NAMD force field.

2.2. Molecular dynamics simulations

The molecular dynamics (MD) simulations were performed in two different steps. First, the receptor binding domain (RBD) bound to the ACE-2 receptor of the host cell (via the 6M0J protein database (pdb) structure, next called RBD_ACE-2) was studied in order to show where are the possible interaction sites between the drugs and/or the nanovector and the protein. The goal of this step was to determine if our system could prevent this main association for the propagation of the virus. The glycosylation of the protein and its steric influence on drug accessibility to the RBD_ACE-2 protein have also been studied recently in the relaxed crystal structures [40].

Then, in a second step, we study the full SARS-CoV-2 spike glycoprotein trimer conformation obtained through the pdb file structure # 6VXX (next called S-trimer). It has a resolution of 2.80 Å from CryoEM (electron microscopy) measurements and corresponds to the closed state of the protein. It can be described by 3 intercalated chains having different domains such as the NTD (N-terminal domain of the SARS-Cov-2 nucleoprotein) and the RBD (Receptor Binding Domain) which belongs to the S_1 part of the protein. Note here that the intercalation of the three chains did not allow us to consider three independent binding processes for each simulation.

Classical MD simulations were performed by building the molecular force field for HCQ and AZM using the SwissParam Force Field Toolkit package. [41,42] When adsorbed on BNO system, the molecular force fields of the system were modified by taking into account the partial charge changes for each atom belonging to the system. These novel partial charges were determined by the Bader formalism of the DFT part as aforementioned.

The protein was studied using the molecular force field according to the CHARMM-GUI procedure which allows proper relaxation of the protein structures [43,44]. Proteins glycosylation was built from CHARMM-GUI Glycolipid Modeler [45].

To study the interaction between the nanovector and the protein, each protein was then associated with a nanovector and solvated in a water box large enough to cancel the protein interaction with its periodic image during the simulation. We generally chose 1.5 nm of water solvent in each direction to separate the protein from the periodic box limit. This prevents interaction with the image of the system in the adjacent cell in periodic boundary conditions applications. To complete the system, NaCl ions (at a concentration of 0.15 M) were added to the water model (transferable intramolecular potential with 3 points, TIP3P). The CHARMM36 force-field optimization parameters were used in all simulations [46]. Complete systems contained 245630, 245681, 245604, 301706, 301877 and 301707 atoms for BN_AZM/RBD_ACE-

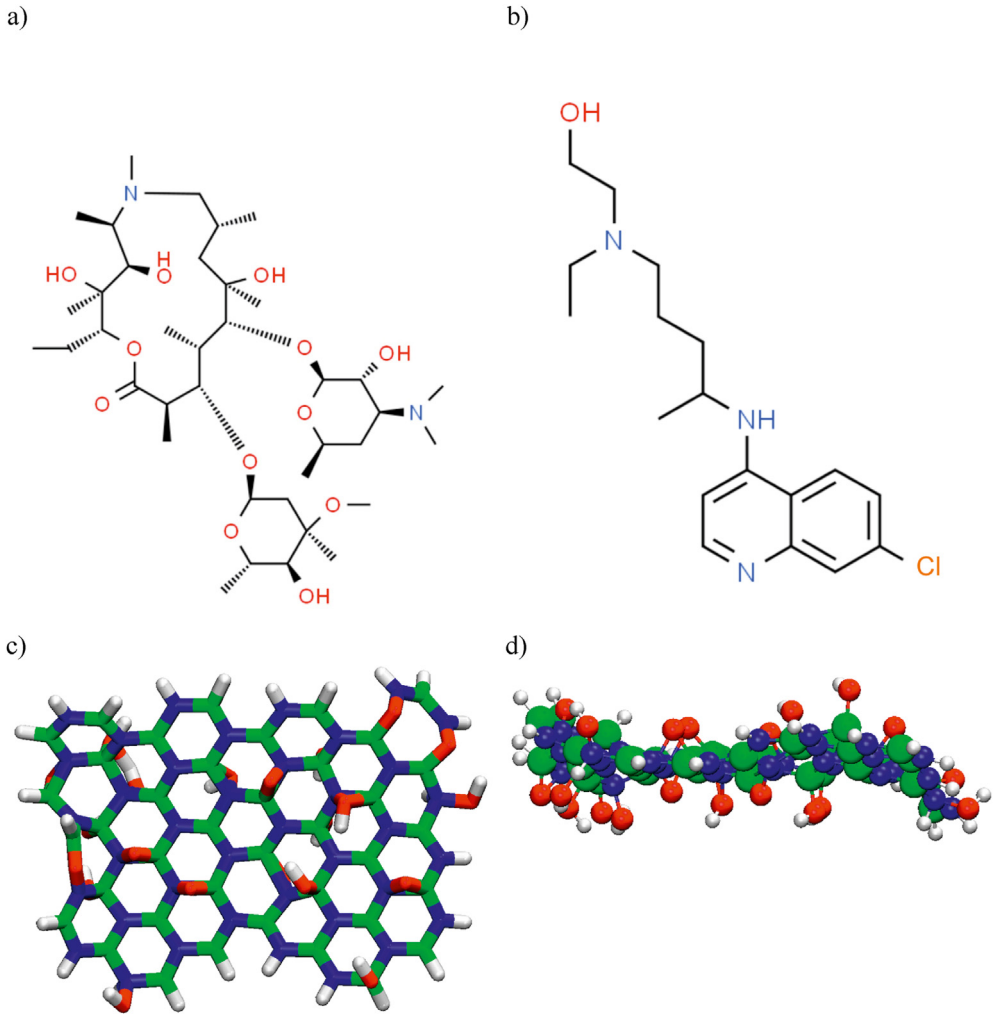

Fig. 1. (a) AZM molecule; (b) HCQ molecule; (c) Top view of BNO; (d) lateral view of BNO (B, N, O, H and Cl atoms are represented as green, blue, red, white and orange spheres, respectively). (For interpretation of the references to color in this figure legend, the reader is referred to the Web version of this article.)

2, BN_HCQ/RBD_ACE-2, AZM_BN_HCQ/RBD_ACE-2, BN_AZM/S-trimer, BN_HCQ/S-trimer and AZM_BN_HCQ/S-trimer systems, respectively.

All the simulations were performed at constant temperature and pressure. The temperature was fixed at 310 K (Langevin dynamics) and the pressure was 1 atm (Langevin piston), respectively. Long-range electrostatic forces were evaluated using the classical particle mesh Ewald (PME) method with 1.2 Å grid spacing, and fourth-order spline interpolation. The integration time step was equal to 1 fs. Each simulation used periodic boundary conditions in the three directions of space. No constraint was imposed during the production phase of the MD simulation. As a consequence, our results were obtained with all atoms left free in the simulation box. Note that for each protein, we first minimized and balanced the structures using MD simulations (NAMD 2.12 package [47]) for 20 ns under biological conditions before studying the entire system in interaction. All protein structures are depicted in Fig. 3a–b.

The possible interaction sites of the nanovector with the proteins were determined through several simulations starting with different configurations obtained by a docking procedure between the viral protein and the nanovectors. For this, we used AutoDock Vina (a fast and accurate evolution of AutoDock) as the molecular docking engine able of producing a large list of ligand positions within a reasonable time. The different starting configurations of the molecular dynamics simulations were chosen according to the best scoring functions obtained in the optimization algorithm. For the RBD_ACE-2, at least 5 different simulations were performed for each drug. For the S-trimer system, only 2 simulations were performed due to the huge size of the system. Note that for each system, an additional simulation where the position of the nanovector was chosen outside the protein surface was performed in order to study the transport path to the active sites of the protein.

3. Results

3.1. Density functional theory

All DFT simulations on AZM/BNO, HCQ/BNO and AZM/BNO/HCQ did not show desorption of hydroxyl or oxo group from the BNO surface. All the data are summarized in Table 1. We find adsorption energy equal to −3.88 eV between the AZM and BNO surface. The Bader charge difference for the AZM molecule between the final state (adsorbed on the nanoflake surface) and the initial state (isolated AZM) gives a total charge transfer equal to 0.08 e^- to the benefit of AZM. In the case of HCQ/BNO, adsorption energy equal to −1.89 eV is obtained. The Bader charge transfer is equal to −0.10 e^- in favor of BNO. In the case of the AZM/BNO/HCQ system, the presence of the two molecules on each side of the BNO

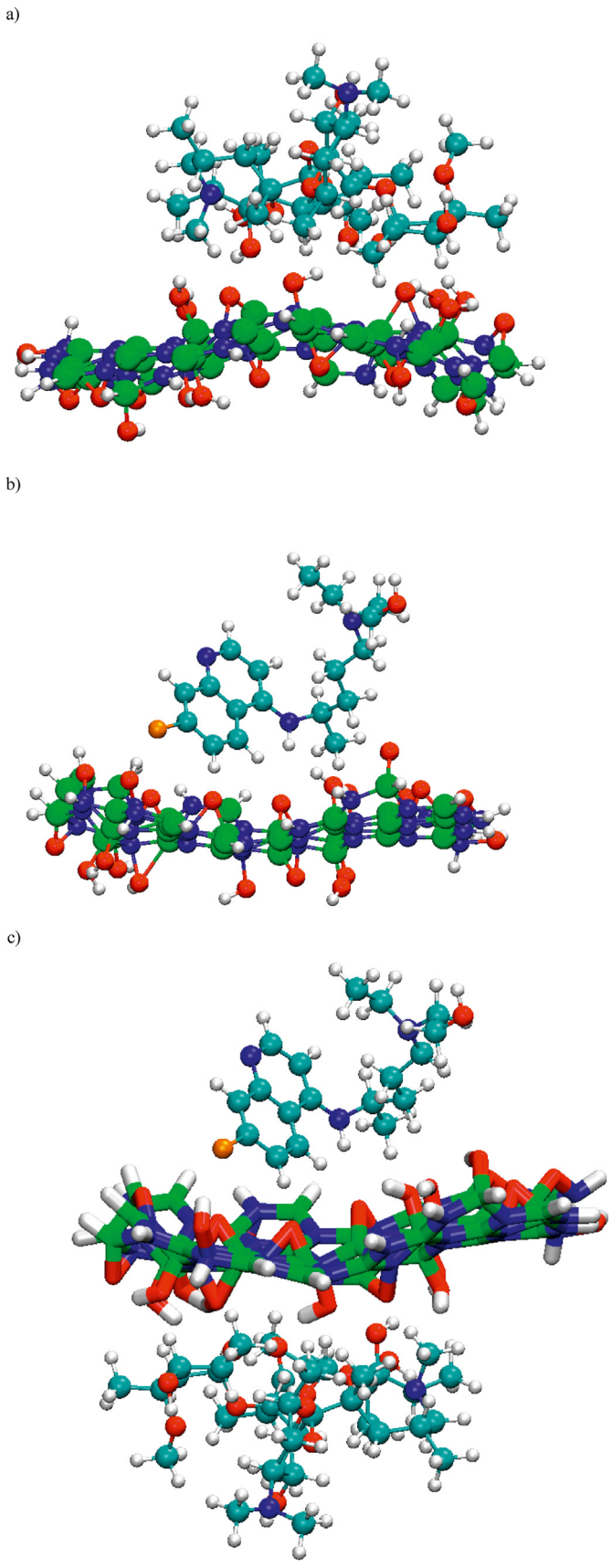

Fig. 2. (a) AZM/BNO system lateral view; (b) lateral view of HCQ/BNO; (c) lateral view AZM/BNO/HCQ (C, B, N, O, H and Cl atoms are represented as cyan, green, blue, red, white and orange spheres, respectively). (For interpretation of the references to color in this figure legend, the reader is referred to the Web version of this article.)

gives −4.86 eV for the adsorption energy of AZM and HCQ on BNO. The Bader charge difference gives a total charge transfer equal to 0.06 e^- and 0.09 e^- to the benefit of AZM and HCQ respectively.

There is a reversible charge transfer between BNO and molecules depending on the system. It is tuned according to its environment.

3.2. Molecular dynamics

3.2.1. Interaction with RBD_ACE-2

Our first investigations were dedicated to the study of drugs and the nanovector with the RBD part of the protein bound to the receptor of the host cell (ACE-2). Due to the large size of the system, the most relevant interaction sites between the drugs, vectorized or not by the BNO, and the protein were determined by docking simulations. Seven configurations were obtained for HCQ/RBD systems with scoring functions ranging from −7.78 to −6.73. For AZM/RBD systems, nine systems exhibited stable scoring functions from −9.94 to −7.52, while five were kept in the case of BNO/RBD system with a scoring function lower than −8. On the basis of these different configurations, molecular dynamics simulations in full solvent were performed. For these simulations, a 1ns equilibration phase was performed before running 10ns of production simulations. The energy between the drug (or nanovector) and the protein was then determined to obtain the most stable site of interaction by molecular dynamics simulation. Additional MD simulation was also performed where the molecules were far from the most stable interaction site. This allows us to verify the steric accessibility of these sites. We have demonstrated that the HCQ molecule could not find any durable interaction site during its diffusion to the RBD_ACE-2 complex whereas several interaction sites were possible by docking. The fluctuant adsorption energies (−26 ± 14 kcal/mol) can explain this desorption. On the contrary, AZM interacts strongly with the protein and can diffuse toward the protein to adsorb on it (−39 ± 6 kcal/mol) [40]. We performed the same calculations with the BNO nanoflake alone. The results depicted in Fig. 4 a,b show a very high level of BNO affinity towards the RBD_ACE-2 complex since the interaction energy rapidly decreases to −167.5 kcal/mol, which is very low compared to any drugs. Note that this energy is the most stable since 2 other over 5 DM simulations based on stable docking sites were not as interesting as in the prediction. It leads to average value equal to −135 ± 30 kcal/mol. The more interacting residues are shown in the zooming views of Fig. 4. We can not determine through these figures any recurrent tendency.

The root mean square deviations (RMSD) of this protein did not show any significant changes whatever the type of molecules since for each one, it converged to a value close to 3 Å (the highest value is obtained for BNO). However, the differences between each system do not seem too significant to be discussed. The most important difference comes from the interaction site. Indeed, while AZM tends to interact with ACE-2, BNO is more particularly adsorbed on the RBD surface. This could explain the behavior of the energy curves between each entity.

As the nanoflake alone can interact strongly with the protein complex, we then studied the role of the nanovectorization of the two drugs with the protein. The interaction energy valleys are shown in Fig. 4b for the vectorization of AZM (black), HCQ (red) and both AZM/HCQ (green) molecules with BNO. While HCQ alone did not find a solution to adsorb onto the complex, we can see in Fig. 4b that BNO can stabilize the drug on the RBD surface with a mean

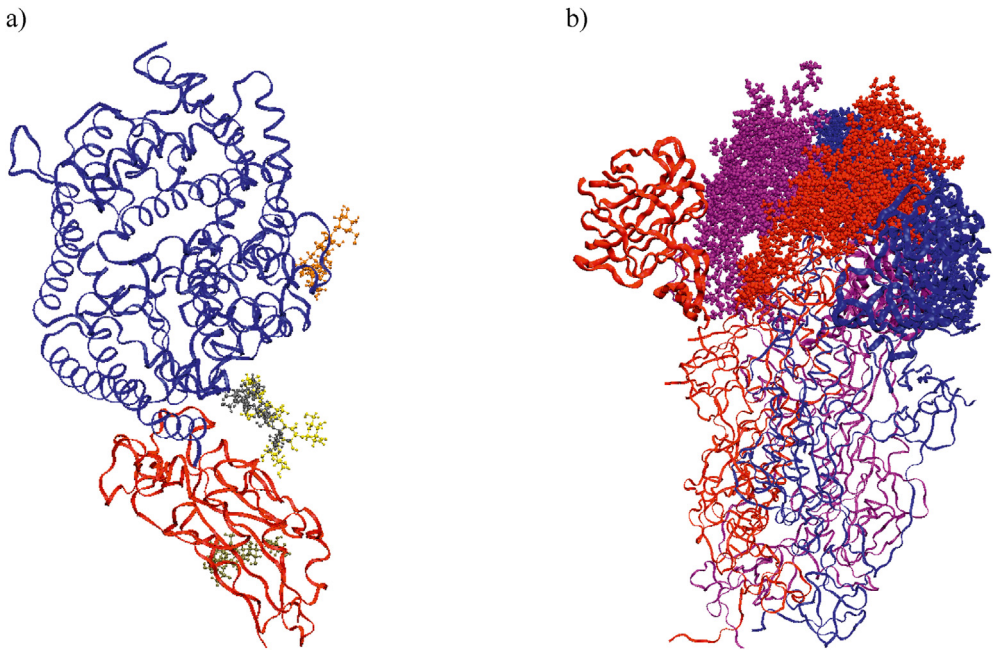

Fig. 3. a) Molecular structure of RBD_ACE-2 (RBD (red)+ACE-2 (blue)) complex with its glycan functions in CPK (Corey-Pauling-Koltun) mode (yellow, orange and gold colors, respectively) representing the different chemical elements by spheres. b) Molecular structure of S-trimer protein. Each monomer is depicted in one color. The RBD parts of the protein were depicted in intense ribbon modes (as for RBD-ACE-2 structures) for the three monomers while the NTD domains appeared in van der Waals spheres and the rest of the protein is depicted in low ribbon modes. (For interpretation of the references to color in this figure legend, the reader is referred to the Web version of this article.)

Table 1
Adsorption energy of molecules on BNO and charge transfer calculated in DFT framework.

	AZM/BNO	HCQ/BNO	AZM/BNO/HCQ
Eads (eV)	−3.88	−1.89	−4.86
Charge transfer for molecule	0.08	−0.10	0.06 (AZM) 0.09 (HCQ)

energy equal to −95 kcal/mol. The site is localized near the RBD/ACE-2 junction (Fig. 4f). Three other configurations, issued from docking calculations confirm that the nanovector can bring the HCQ on the RBD but with a lower interaction energy (equal to −40 ± 15 kcal/mol). The nanovectorization of AZM also increases its affinity for the protein compared to AZM alone. Indeed, the interaction energy obtained for this nanovector converges to −110 kcal/mol, far below the interaction energies of the drug alone. Five other configurations were tested leading to energy varying from −65 to −107 kcal/mol. Note that the best interaction site is now on the ACE-2 protein. We can underline that the behavior of the two complexes is quite different. In fact, the HCQ faces the protein when the nanovector is adsorbed while it is the BNO surface that interacts directly with the protein during the transport of the AZM molecule. Note that the nanovector which aims to transport the two molecules at the same time did not work in this study. It leads to drug repulsion toward the complex protein as observed for the HCQ molecule. We extracted from all simulation runs the specific interaction energy of the vectorized drug with the protein. For HCQ, this leads to a pair interaction ranging from −20 to −70 kcal/mol, the most stable corresponding to Fig. 4f. Indeed, in this position, the BNO tends to force the molecule to adopt a specific configuration that also improves its interaction with the protein. For AZM, the results are less convincing since it leads to an interaction energy that converges to at most −6 kal/mol. Note however, that in a particular case (where the total energy of the vector was only −78 kcal/mol) the interaction of the vectorized AZM converges to −40 kcal/mol.

3.2.2. Interaction with the full protein (S-trimer)

We have studied the interaction of our different nanovectors with the closed part of the viral protein (S-trimer). Both HCQ and AZM drugs can find through diffusion an interaction site with this part of the virus. The energy resulting from these adsorptions leads to the same value close to −30 kcal/mol (Fig. 5a) as in the case of the RBD_ACE-2 complex. Other sites simulated with DM and whose starting point was determined by docking simulations, did not reveal lowest interaction energy. The BNO nanoflake alone can also interact with the S-trimer since its energy, once stabilized on it, converges to about −100 kcal/mol. This value is still much lower than for any drugs. All the entities adsorb near the RBD site of the protein. For the S-trimer, RBD is in its close form. The molecules can thus also find a stable adsorption site in this case as in the open state of the RBD (when attached to the ACE-2 receptor). We did not find any significant recurring residue which could explain the position of the molecules here. The RMSD of this protein complex remains the same for each molecule, it tends to a value close to 3 Å (the highest value is obtained for BNO). The differences between each system are again not so large to be significant.

The interaction of the nanovector made of BNO combined to one or two drugs with the S-trimer structure was then evaluated. The interaction energy valleys depicted in Fig. 5b show that each nanovector can adsorb close to the protein with an adsorption energy which is equivalent for the three studied systems (about −65 ± 5 kcal/mol). While BNO (drug, respectively) alone adsorbed on the complex with a smaller (higher, respectively) energy, we can see in Fig. 5b that using BNO as a nanovector allowed to better stabilize each drug with the S-trimer surface. The pair interaction of the vectorized drug with the protein tends to −22 ± 4 kcal/mol, a value slightly higher than without BNO. Nanovectorization is however slightly different in terms of adsorption velocity. When both drugs are vectorized with BNO, the

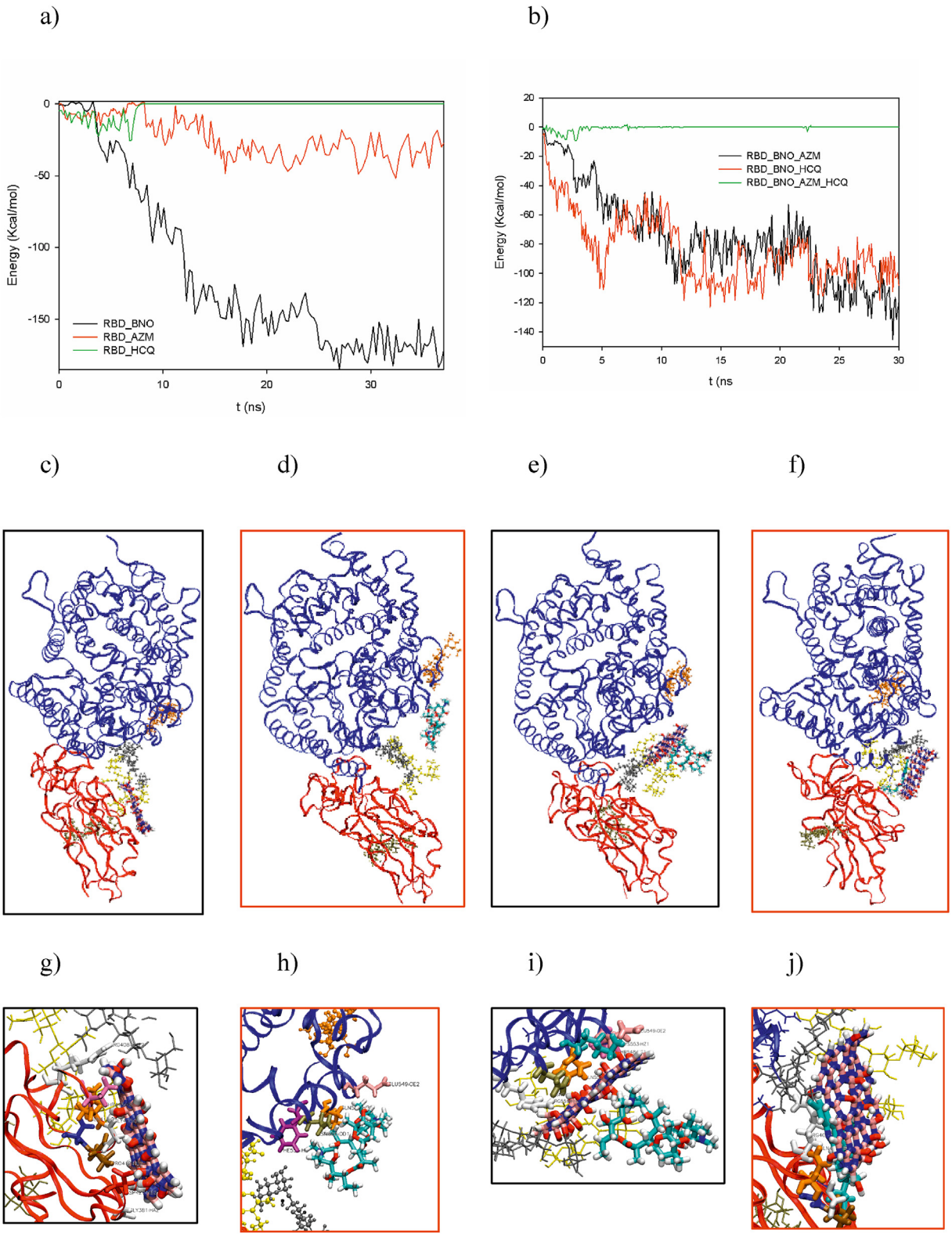

Fig. 4. a) Interaction energy of BNO (black), AZM (red) and HCQ (green) molecules with RBD_ACE-2 complex. b) Interaction energy of the different nanovectors (BNO/AZM (black), BNO/HCQ (red) and AZM/BNO/HCQ (green) with RBD_ACE-2 complex. c) (d,e,f) Position of BNO (AZM, BNO/AZM, BNO/HCQ, respectively) at the end of the simulation. g) (h,i,j) Zoom of the BNO (AZM, BNO/AZM, BNO/HCQ, respectively) position at the end of the simulation. The residues of the protein that show the most important contribution to the interaction energy are depicted in these last figures. (For interpretation of the references to color in this figure legend, the reader is referred to the Web version of this article.)

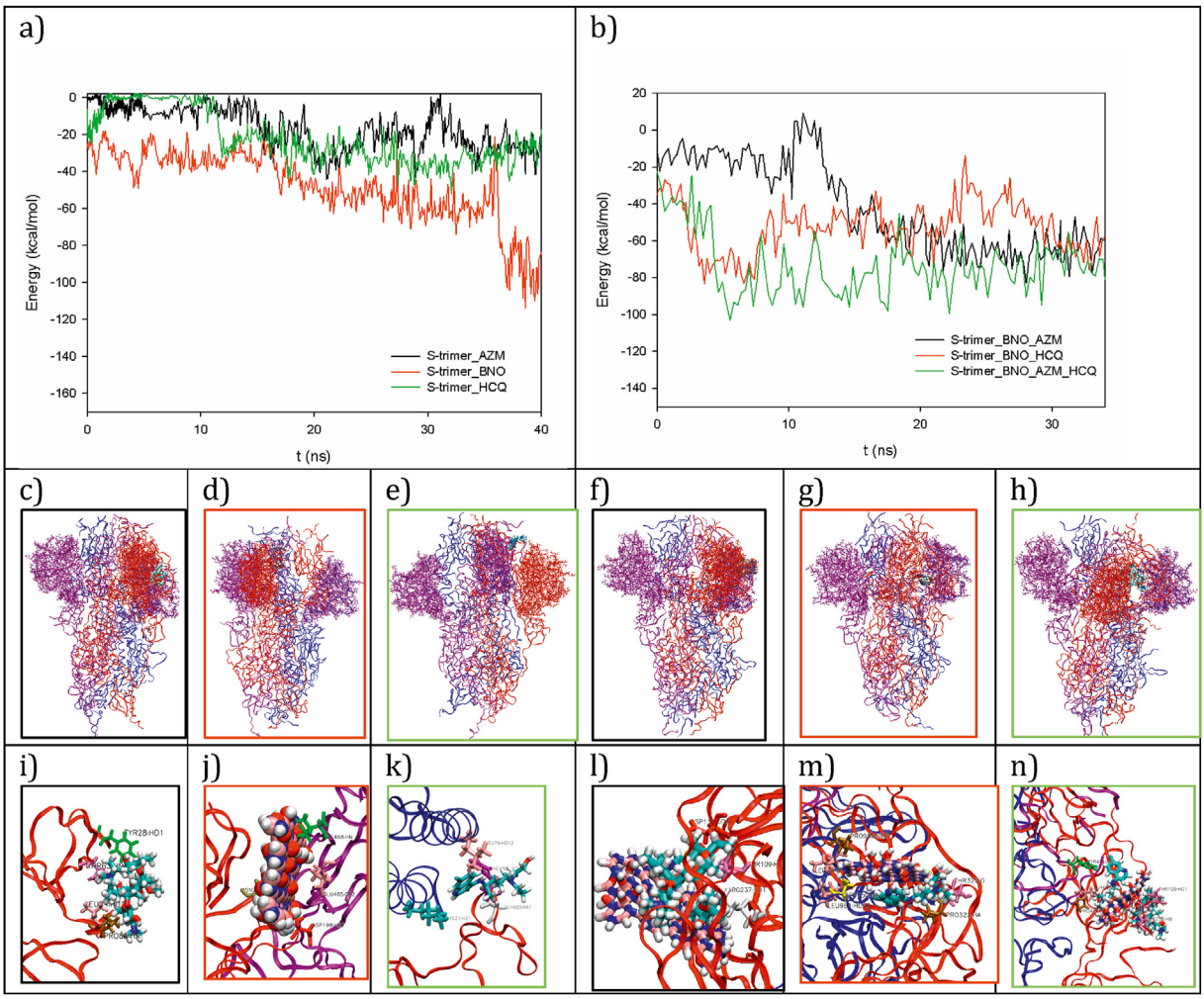

Fig. 5. a) Interaction energy of BNO (red), AZM (black) and HCQ (green) molecules with S-trimer protein. b) Interaction energy of the different nanovector (BNO/AZM (black), BNO/HCQ (red) and AZM/BNO/HCQ (green)) with S-trimer protein. c) (d,e,f,g,h) Position of AZM (BNO, HCQ, BNO/AZM, BNO/HCQ, BNO/AZM/HCQ, respectively) at the end of the simulation. g) (h,i,j) Zoom of the AZM (BNO, HCQ, BNO/AZM, BNO/HCQ, BNO/AZM/HCQ, respectively) position at the end of the simulation. The residues of the protein that show the most important contribution to the interaction energy are depicted in these last figures. (For interpretation of the references to color in this figure legend, the reader is referred to the Web version of this article.)

adsorption site was obtained faster than when only one drug was transported on the vector. The interaction sites are always located in the same place for the three complexes. Of course, the latter depends on the initial position of the molecules that were chosen in an equivalent manner to accommodate close to the best docking score site. Some other interaction sites are possible on this large protein and two more have been tested based on docking simulations. We did not observe with these two supplementary simulations another more stable site. It should be noted that the search for the lower interaction site is not the main goal of these studies since we aimed to prove that the nanovector improved the drug affinity for the viral protein.

4. Discussion

Recently, MD simulations have shown that HCQ and AZM aim to block the interaction of RBD with the cell receptor and more particularly with the gangliosides [49]. Indeed, each drug being adsorbed specifically on different targeted sites, the virus attack toward the cell receptor would be efficiently blocked [50]. More, this would improve the treatment of the disease since the two drugs act synergistically on the viral protein [50,51].

Our studies have not shown any real interaction between HCQ molecules and RBD in its opened conformation. However, with the closed state of the viral protein, HCQ can find a way to adsorb on it. For AZM, the interaction energies appear equivalent whatever the simulated target. The influence of the BNO, used as a nanovector is much more interesting. Indeed, its strong interaction with either the open receptor binding domain (RBD) or the closed state structure of the protein makes its use very efficient against the SARS-Cov-2 virus. By comparing the interaction energies of different molecules alone, whatever the protein studied, BNO exhibited an energy at least 3 to 4 times lower than the drug one but is not known to have any therapeutic effect. However, due to its hydrophobic properties, its diffusion to the target is greatly improved at room temperature compared to the attachment of the therapeutic agents with the protein.

When used as a nanovector, the behavior of the nanoflake is not disturbed by the presence of the drug molecules (unless both molecules were adsorbed on both sides of the nanosheet). The drug nanovector, due to the strong affinity of BNO for the proteins, adsorbs on the different proteins (even if the drug alone could not). For instance, HCQ which is not attracted to the RBD_ACE-2 structure, can diffuse there when it is transported by the BNO nanoflake.

The energies obtained in each case present comparable values (although slightly higher) to the interaction of the BNO alone with the protein and those of the drugs alone. More, for HCQ, the important attraction of BNO to the protein forces the drug to penetrate deeply into the protein. It thus improves the affinity of HCQ for the virus since we have not found any stable state where HCQ diffused alone. For AZM, most of our simulations show an improvement of the drug transport but a decrease in the direct drug interaction with the protein. The nanosheet, in its more stable site, faces the residues of the protein and does not allow AZM to be in an optimized position regarding the protein. The size of the system is probably at the origin of this result but one of our simulations shows however that a configuration could be found where AZM is in full interaction with the protein. The use of BNO as a nanovector thus slightly decreases its affinity for the virus but makes it possible to stabilize the drug on the different proteins with a rapid transfer from the vector to the protein. It can thus answer to the problem of the medical dose in case of dual therapy using HCQ plus AZM treatment since the target of this drug will be more easily reached. As a consequence, the nanovectorization of the drugs by the biocompatible BNO surface improves the drug targeting, allowing dose reduction if necessary. Analyses of the different residues responsible for the adsorption of the compound on the protein highlights that the major part of the interaction comes from electrostatic contributions.

Although this study is not exhaustive (all the adsorption states have not been systemically studied while several have been tested), we demonstrate the strong affinity of the nanovector with the viral proteins, and prove by these calculations that the BNO surface could impose the way of drug vectorization. It should be noted however that this study should be improved to be fully exhaustive. Indeed, to demonstrate quantitatively that BNO could effectively transport the drug accurately, longer flooding simulations of the protein in the presence of a higher concentration of drug (with or without BNO) would have to be performed. This is outside the scope of this first proof of concept since this approach would require significant computational resources.

5. Conclusion

In this period troubled by the pandemic, researchers are looking for an efficient treatment against the SARS-Cov-2 virus. Several treatments have been tested but now, no real one has emerged. Dual therapy consisting of hydroxychloroquine molecules plus azythromicin has proved to be effective, but the doses of drugs needed to answer to the disease could give to patients some important side effects. Using combined quantum and dynamic numerical simulations, the adsorption of these drugs on biocompatible boron nitride oxide nanosheet was possible in a very stable way. Our calculations demonstrated that the strong affinity of the BNO surface towards different parts of the viral protein in its closed or open structures can help the drug to be adsorbed onto the protein. Indeed, the nanovectorization of these drugs using BNO helps the drugs to diffuse rapidly to the viral protein and in some cases improves (HCQ in particularly) the interaction of the drugs with the virus. For the future, we hope that our results can reinforce the research community on the use of the BNO nanovector for the delivery of therapeutic agents in the fight against coronavirus.

Declaration of competing interest

The authors declare that they have no known competing financial interests or personal relationships that could have appeared to influence the work reported in this paper.

Acknowledgements

Calculations were performed at the supercomputer regional facility Mesocentre of the University of Franche-Comté with the assistance of K. Mazouzi. This work was granted access to the HPC resources of IDRIS, Jean Zay supercomputer, under the allocation 2020 - DARI AP010711661 made by GENCI. We would like to express our gratitude to the IDRIS team (S. Requena, P.-F. Lavallée, R. Lacroix and S. Van Crienkingen), which was able to be very reactive to our request in a very tense pandemic climate, without whom this work would not have been possible.

References

[1] P.S. Masters, Adv. Virus Res. 66 (2006) 193–292.
[2] S.R. Weiss, S. Navas-Martin, Microbiol. Mol. Biol. Rev. 69 (2005) 635–664.
[3] V. Coronaviridae Study Group of the International Committee on Taxonomy of, Nature microbiology, 2020, 5, 536–544.
[4] F. Wu, S. Zhao, B. Yu, Y.-M. Chen, W. Wang, Z.-G. Song, Y. Hu, Z.-W. Tao, J.-H. Tian, Y.-Y. Pei, M.-L. Yuan, Y.-L. Zhang, F.-H. Dai, Y. Liu, Q.-M. Wang, J.-J. Zheng, L. Xu, E.C. Holmes, Y.-Z. Zhang, Nature 579 (2020) 265–269.
[5] P. Zhou, X.L. Yang, X.G. Wang, B. Hu, L. Zhang, W. Zhang, H.R. Si, Y. Zhu, B. Li, C.L. Huang, H.D. Chen, J. Chen, Y. Luo, H. Guo, R.D. Jiang, M.Q. Liu, Y. Chen, X.R. Shen, X. Wang, X.S. Zheng, K. Zhao, Q.J. Chen, F. Deng, L.L. Liu, B. Yan, F.X. Zhan, Y.Y. Wang, G.F. Xiao, Z.L. Shi, Nature 579 (2020) 270–273.
[6] N. Chen, M. Zhou, X. Dong, J. Qu, F. Gong, Y. Han, Y. Qiu, J. Wang, Y. Liu, Y. Wei, J.a. Xia, T. Yu, X. Zhang, L. Zhang, Lancet 395 (2020) 507–513.
[7] F. Li, Ann. Rev. Virol. 3 (2016) 237–261.
[8] B.J. Bosch, R. van der Zee, C.A.M. de Haan, P.J.M. Rottier, J. Virol. 77 (2003) 8801–8811.
[9] W. Song, M. Gui, X. Wang, Y. Xiang, PLoS Pathog. 14 (2018) e1007236.
[10] W. Li, M.J. Moore, N. Vasilieva, J. Sui, S.K. Wong, M.A. Berne, M. Somasundaran, J.L. Sullivan, K. Luzuriaga, T.C. Greenough, H. Choe, M. Farzan, Nature 426 (2003) 450–454.
[11] M. Gui, W. Song, H. Zhou, J. Xu, S. Chen, Y. Xiang, X. Wang, Cell Res. 27 (2017) 119–129.
[12] J. Kouznetsova, W. Sun, C. Martínez-Romero, G. Tawa, P. Shinn, C.Z. Chen, A. Schimmer, P. Sanderson, J.C. McKew, W. Zheng, A. García-Sastre, Emerg. Microb. Infect. 3 (2014) e84.
[13] S. He, B. Lin, V. Chu, Z. Hu, X. Hu, J. Xiao, A.Q. Wang, C.J. Schweitzer, Q. Li, M. Imamura, N. Hiraga, N. Southall, M. Ferrer, W. Zheng, K. Chayama, J.J. Marugan, T.J. Liang, Sci. Transl. Med. 7 (2015), 282ra249-282ra249.
[14] N.J. Barrows, R.K. Campos, S.T. Powell, K.R. Prasanth, G. Schott-Lerner, R. Soto-Acosta, G. Galarza-Muñoz, E.L. McGrath, R. Urrabaz-Garza, J. Gao, P. Wu, R. Menon, G. Saade, I. Fernandez-Salas, S.L. Rossi, N. Vasilakis, A. Routh, S.S. Bradrick, M.A. Garcia-Blanco, Cell Host Microbe 20 (2016) 259–270.
[15] H.-H. Fan, L.-Q. Wang, W.-L. Liu, X.-P. An, Z.-D. Liu, X.-Q. He, L.-H. Song, Y.-G. Tong, Chin. Med. J. 133 (2020) 1051–1056.
[16] B. Cao, Y. Wang, D. Wen, W. Liu, J. Wang, G. Fan, L. Ruan, B. Song, Y. Cai, M. Wei, X. Li, J. Xia, N. Chen, J. Xiang, T. Yu, T. Bai, X. Xie, L. Zhang, C. Li, Y. Yuan, H. Chen, H. Li, H. Huang, S. Tu, F. Gong, Y. Liu, Y. Wei, C. Dong, F. Zhou, X. Gu, J. Xu, Z. Liu, Y. Zhang, H. Li, L. Shang, K. Wang, K. Li, X. Zhou, X. Dong, Z. Qu, S. Lu, X. Hu, S. Ruan, S. Luo, J. Wu, L. Peng, F. Cheng, L. Pan, J. Zou, C. Jia, J. Wang, X. Liu, S. Wang, X. Wu, Q. Ge, J. He, H. Zhan, F. Qiu, L. Guo, C. Huang, T. Jaki, F.G. Hayden, P.W. Horby, D. Zhang, C. Wang, N. Engl. J. Med. 382 (2020) 1787–1799.
[17] A.B. Zakaria, F. Picaud, E. Duverger, X. Devaux, E. Delabrousse, T. Gharbi, O. Micheau, G. Herlem, Chem. Phys. Lett. 633 (2015) 273–281.
[18] M. El Khalifi, E. Duverger, H. Boulahdour, F. Picaud, Anal. Meth. 7 (2015) 10145–10150.
[19] J. Bentin, E. Duverger, F. Picaud, J. Mol. Model. 25 (2019) 72.
[20] E. Duverger, T. Gharbi, E. Delabrousse, F. Picaud, Phys. Chem. Chem. Phys. 16 (2014) 18425–18432.
[21] M. El Khalifi, E. Duverger, T. Gharbi, H. Boulahdour, F. Picaud, Anal. Meth. 8 (2016) 1367–1372.
[22] E. Duverger, S. Balme, M. Bechelany, P. Miele, F. Picaud, Appl. Surf. Sci. 475 (2019) 666–675.
[23] E. Duverger, F. Picaud, L. Stauffer, P. Sonnet, ACS Appl. Mater. Interfaces 9 (2017) 37554–37562.
[24] Q. Weng, B. Wang, X. Wang, N. Hanagata, X. Li, D. Liu, X. Wang, X. Jiang, Y. Bando, D. Golberg, ACS Nano 8 (2014) 6123–6130.
[25] Q. Weng, X. Wang, X. Wang, Y. Bando, D. Golberg, Chem. Soc. Rev. (2016) 3989–4012.
[26] P. Hohenberg, W. Kohn, Phys. Rev. 136 (1964) 864–871.
[27] W. Kohn, L.J. Sham, Phys. Rev. 140 (1965) 1133–1138.
[28] P. Ordejon, E. Artacho, J.M. Soler, Phys. Rev. B 53 (1996) 10441–10444.
[29] J.M. Soler, E. Artacho, J.D. Gale, A. García, J. Junquera, P. Ordejón, D. Sánchez-Portal, J. Phys. Condens. Matter 14 (2002) 2745–2779.
[30] M. Dion, H. Rydberg, E. Schröder, D.C. Langreth, B.I. Lundqvist, Phys. Rev. Lett. 92 (2004) 246401.

[31] J.P. Perdew, K. Burke, M. Ernzerhof, Phys. Rev. Lett. 77 (1996) 3865–3868.
[32] G. Román-Pérez, J.M. Soler, Phys. Rev. Lett. (2009) 103, 096102.
[33] T. Sainsbury, A. Satti, P. May, Z. Wang, I. McGovern, Y.K. Gun'ko, J. Coleman, J. Am. Chem. Soc. 134 (2012) 18758–18771.
[34] D. Lee, B. Lee, K.H. Park, H.J. Ryu, S. Jeon, S.H. Hong, Nano Lett. 15 (2015) 1238–1244.
[35] Y. Lin, T.V. Williams, J.W. Connell, J. Phys. Chem. Lett. 1 (2010) 277–283.
[36] A. Bagri, C. Mattevi, M. Acik, Y.J. Chabal, M. Chhowalla, V.B. Shenoy, Nat. Chem. 2 (2010) 581–587.
[37] X. Fan, W. Peng, Y. Li, X. Li, S. Wang, G. Zhang, F. Zhang, Adv. Mater. 20 (2008), 4490)4493.
[38] R.F.W. Bader, Chem. Rev. 91 (1991) 893–928.
[39] G. Henkelman, A. Arnaldsson, H. Jonsson, Comput. Mater. Sci. 36 (2006) 354–360.
[40] F. Picaud, G. Herlem, Austin J. Nanomed. Nanotechnol. 9 (1) (2021) 1061.
[41] V. Zoete, M.A. Cuendet, A. Grosdidier, O. Michielin, J. Comput. Chem. 32 (2011) 2359–2368.
[42] C.G. Mayne, J. Saam, K. Schulten, E. Tajkhorshid, J.C. Gumbart, J. Comput. Chem. 34 (2013) 2757–2770.
[43] S. Jo, X. Cheng, S.M. Islam, L. Huang, H. Rui, A. Zhu, H.S. Lee, Y. Qi, W. Han, K. Vanommeslaeghe, A.D. MacKerell, B. Roux, W. Im, in: T. Karabencheva-Christova (Ed.), Advances in Protein Chemistry and Structural Biology, vol. 96, 2014, pp. 235–265. Academic Press.
[44] S. Jo, T. Kim, V.G. Iyer, W. Im, J. Comput. Chem. 29 (2008) 1859–1865.
[45] J. Lee, D.S. Patel, J. Ståhle, S.J. Park, N.R. Kern, S. Kim, J. Lee, X. Cheng, M.A. Valvano, O. Holst, Y.A. Knirel, Y. Qi, J. Sunhwan, B. Jeffery, G. Widmalm, I. Wonpil, J. Chem. Theor. Comput. 15 (2019) 775–786.
[46] R. Best, X. Zhu, J. Shim, P. Lopes, J. Mittal, M. Feig, A. MacKerell, J. Chem. Theor. Comput. 8 (2012) 3257–3273.
[47] J.C. Phillips, R. Braun, W. Wang, J. Gumbart, E. Tajkhorshid, E. Villa, C. Chipot, R.D. Skeel, L. Kalé, K. Schulten, J. Comput. Chem. 26 (2005) 1781–1802.
[49] M. Matrosovich, G. Herrler, H.D. Klenk, in: R. Gerardy-Schahn, P. Delannoy, M. von Itzstein (Eds.), Top Current Chemistry, Springer International Publishing, 2015, pp. 1–28. Cham.
[50] J. Fantini, H. Chahinian, N. Yahi, Int. J. Antimicrob. Agents (2020) 106020.
[51] J. Fantini, C. Di Scala, H. Chahinian, N. Yahi, Int. J. Antimicrob. Agents 55 (2020) 105960.